A dynamic three-layer model of the global overturning circulation

Tom Beucler*

Program in Atmospheres, Oceans and Climate, Massachusetts Institute of Technology, Cambridge, MA 02139, USA

*Correspondence to: Tom Beucler, MIT, 77 Massachusetts Ave — 54-1815, Cambridge, MA 02139, USA.
E-mail: tom.beucler@gmail.com

Received . . .

1. Introduction

The global ocean is connected from pole to pole by a three-dimensional global overturning circulation (GOC) that transports heat, freshwater, carbon, salt, etc. over long timescales (Ganachaud and Wunsch 2003; Toggweiler 1999). A first understanding of the GOC (cf figure 1) comes from taking a zonal average of the oceanic circulation along isopycnals (surfaces of constant density). Observations (eg (Lumpkin and Speer 2007; Talley 2008; Ganachaud and Wunsch 2000)) show the coexistence of two cells:

1. An upper cell, driven by the convection of dense waters near the North Pole, upwelling along isopycnals in the Southern Ocean, and weak diapycnal mixing at middle and low latitudes.
2. A lower cell, with sinking around the Antarctic continent, and strong diapycnal mixing at middle and low latitudes.

The Southern Ocean is a crucial part of the GOC (eg (Marshall and Speer 2012; Jones et al. 2011)): Its strong eastwards surface winds allow the return of deep and abyssal waters to the surface through Ekman pumping; at the same time, they steepen isopycnals and generate baroclinic eddies that transform surface and deep waters into deep and abyssal waters. A full understanding of the GOC requires to acknowledge its three dimensional structure (Talley 2013): not only are the two cells connected in a single basin, but also between different basins, through the inter-basin exchange around the Antarctic continent (cf figure 5). The GOC can thus be seen as a single loop, spanning the convectively-driven Atlantic basin and the mixing-driven Indo-Pacific basin. Multiple models of the GOC exist in the litterature (eg (Gnanadesikan 1999; Nikurashin and Vallis 2011, 2012; Shakespeare and McC. Hogg 2012)), but none of them simultaneously include:

1. A simple representation of the deep and abyssal stratification.
2. Dynamical equations to resolve the evolution of the GOC and the ocean stratification in time, in response to a climatic change.
3. The zonal inter-basin exchange through the Southern Ocean.

Our model, built on first principles, addresses these three points to provide a basic understanding of the GOC, that can be tested against observations and general circulation models (GCM). We build a one basin (section 2.1) and two basins (section 3.1) three layer model of the GOC. We then use this model to understand the dynamics of the stratification in response to a given climate change (sections 2.2 and 3.2). Finally, we are able to formulate a simple heat uptake model based on the advective timescales of the GOC (sections 2.3 and 3.3).

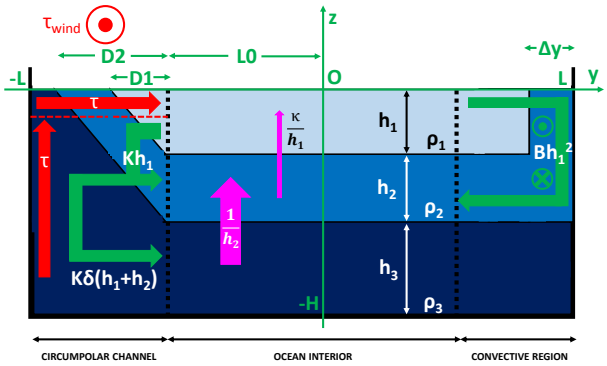

Figure 1. Three layer model of the global overturning circulation. The transports are indicated in dimensionless form.

2. Three layer model of a single basin

2.1. *Model setup*

Following figure 1, we represent the ocean by a rectangular box of length $2L$ and depth H with:

1. In the vertical: Three layers (intermediate, deep and abyssal waters) of thicknesses (h_1, h_2, h_3) and constant densities (ρ_1, ρ_2, ρ_3).
2. In the North-South direction: A circumpolar channel extending from the South Pole $y = -L$ to its Northern edge $y = -L_0$, where the mean isopycnals are sloped; an ocean basin extending from $y = -L_0$ to $y = L_0$; a polar convective zone extending from $y = L_0$ to the North pole $y = L$. By construction of the model, the circumpolar channel and the Polar convective zone have the same meridional extent.

We make the following assumptions about the two mean isopycnals:

1. The first isopycnal, separating layers 1 and 2, outcrops southerly at a distance D_1 from the Northern edge of the circumpolar channel, imposed by atmospheric boundary conditions; its (negative) slope there is given by $\alpha_1 = -h_1 D_1^{-1}$. Polar convection brings it almost vertically back to the surface in the northern latitudes, where it outcrops again.
2. The second isopycnal, separating layers 2 and 3, outcrops southerly at a distance D_2 from the Northern edge of the circumpolar channel, imposed by atmospheric boundary conditions; its (negative) slope there is given by $\alpha_2 = -(h_1+h_2) D_2^{-1}$. However, it does not outcrop in the northern latitudes.

2.1.1. *Dynamics in the circumpolar channel*

For simplicity sake, we assume that eastwards winds exert a constant stress $\tau(y)$ at the surface of the circumpolar channel, while the surface of the ocean basin is stress-free. This distribution of stress induces a vertical transport from the depths to the surface of the circumpolar channel (Ekman upwelling), and a meridional transport from the South to the North of the channel (Ekman transport). Baroclinic instability prevents the mean isopycnal to outcrop vertically, meaning that eddy-transport counteracts the Ekman upwelling by transporting water from the surface to the depth of the circumpolar channel. The residual circulation is the sum of the two counter-acting transports. By using a Transformed Mean Eulerian framework that does not assume geostrophy (eg (Plumb and Ferrari 2005)), and using Gent and McWilliams's closure for the eddy fluxes (Gent and McWilliams 1990), we can make this sum apparent in the residual circulations $\psi_i^\dagger$ from layer i to layer $(i+1)$:

$$\psi_i^\dagger(y) = \underbrace{-\frac{\tau(y)}{\rho_0 f(y)}}_{\text{wind}} + \underbrace{K_{\text{eddy}}\alpha_i}_{\text{eddies}},\ i=1,2, \tag{1}$$

where ρ_0 is the mean density of seawater, f the Coriolis parameter and K_{eddy} is the lateral eddy diffusivity. The value $\psi_i^\dagger(y=-L_0)$ of these streamfunctions at the Northern edge of the circumpolar channel is then simply obtained by evaluating the wind-stress and the (negative) Coriolis parameter at this latitude:

$$\tau_0 \overset{\text{def}}{=} \tau(y=-L_0), \tag{2}$$

$$-f_0 \overset{\text{def}}{=} f(y=-L_0) = -2\Omega\sin(\frac{L_0}{a}). \tag{3}$$

We have introduced the Earth's radius a and rotation rate Ω.

2.1.2. *Dynamics in the polar convecting zone*

To evaluate the Atlantic transport near the North Pole, where the water convects from the upper layer to the lower layer, we make three assumptions:

1. As we are interested in large-scale flows, the Rossby number is small and geostrophy applies:

$$\rho_0 f \begin{pmatrix} v_i \\ -u_i \end{pmatrix} = \begin{pmatrix} \frac{\partial}{\partial x} \\ \frac{\partial}{\partial y} \end{pmatrix} p_i,\ i=1,2, \tag{4}$$

where (u_i, v_i, p_i) are respectively the zonal velocity, meridional velocity, and pressure of layer i, and (x,y) are the zonal and meridional coordinates.

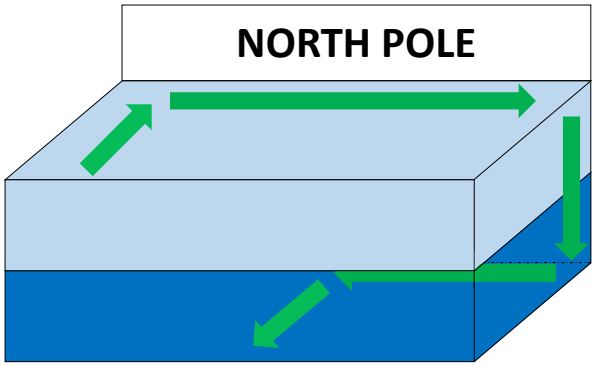

Figure 2. Polar circulation in the three layer model. As a strong northwards western boundary current arrives to the Pole, it is deviated eastwards by the southwards buoyancy gradient through the thermal wind relation. At this latitude, the atmosphere cools the surface water, and make it sink to the deep ocean, where it is deviated westwards by the southwards buoyancy gradient. Finally, the flow returns southwards in the lower layer.

2. Except at the precise zone where water convects, we neglect the rate of change of the vertical velocities in the flow and hydrostasy applies:

$$\frac{\partial p_i}{\partial z} = -\rho_i g,\ i=1,2,3, \tag{5}$$

where z is the vertical coordinate, g the gravity constant and ρ_i the density of layer i.
3. Following figure 1, we assume that the abyssal layer is motionless ($u_3 = v_3 = 0$) because it does not outcrop in the Northern hemisphere (for example, the 27.9kg.m^{-3} neutral density surface is a good candidate for the isopycnal separating the deep and abyssal layers). Following figure 2, we also assume that the transport in the upper layer is equal and opposite to the transport in the deep layer. To compute transports in this model, we neglect the variations of the density in the vertical, so that the previous statement about the mass fluxes also applies for the volume fluxes:

$$h_1 \begin{pmatrix} u_1 \\ v_1 \end{pmatrix} + h_2 \begin{pmatrix} u_2 \\ v_2 \end{pmatrix} = \begin{pmatrix} 0 \\ 0 \end{pmatrix}. \tag{6}$$

If we assume that the flow is geostrophic and has similar velocities in the upper and deep layers, the resulting transport is complicated (see appendix A). Here, we assume that only the upper layer is dynamically active because it is very thin ($h_1 \ll h_2, h_3$). The lower layer, which contains the return flow of the upper layer according to equation 6, is approximated as being so deep that v_2 is negligible, meaning that its pressure p_2 has no horizontal gradients. Applying the dynamical condition $0 = (p_2 - p_1)(x,y,z=-h_1)$, the pressure of the upper layer is then given by:

$$p_1(x,y,z) = \rho_0 g_1' h_1(x,y) - \rho_1 g z. \tag{7}$$

We have introduced the buoyancy contrast (reduced gravity) between a layer i and a layer $(i+1)$:

$$g_i' \overset{\text{def}}{=} g\frac{\rho_{i+1}-\rho_i}{\rho_0},\ i=1,2. \tag{8}$$

Note that the previous approximation is only made for the sake of simplicity, and that we will compare our results to those obtained if the more rigorous approach of appendix A is adopted. Combining equations (4) and (7) allows us to compute the Eastwards flow in the upper layer:

$$u_1 = -\frac{g_1'}{f}\frac{\partial h_1}{\partial y} > 0. \tag{9}$$

The total zonal (and meridional according to equation 6) transport is given by:

$$h_1 u_1 = -\frac{g_1'}{2f}\frac{\partial h_1^2}{\partial y}, \tag{10}$$

and the total polar circulation at ($y = L_0$) scales like:

$$\psi^p(y = L_0) \sim \frac{\varepsilon g_1'}{2f}\frac{h_1^2}{\Delta y}, \tag{11}$$

where we have introduced the factor ε to account for the fact that only a fraction of the ocean (the Atlantic ocean) is open to the North and undergoes polar convection. Δy is the typical meridional distance over which the water becomes denser and convects.

2.1.3. *Buoyancy balance in the ocean interior*

In the ocean interior, the isopycnals are flat and we only have a steady diapycnal (across surfaces of constant density) advection-diffusion balance of buoyancy b:

$$\frac{\partial \psi}{\partial y}\frac{\partial b}{\partial z} \approx \kappa_i \frac{\partial^2 b}{\partial z^2} \tag{12}$$

In (12), we neglect the tendency of the diapycnal diffusivity for the sake of simplicity but recognize that it can affect the sensitivity of the GOC to Southern wind changes (eg (Mashayek et al. 2015)). Writing this balance from one edge of the ocean ($y = -L_0$) to the other ($y = L_0$), we obtain:

1. Vertically integrating from the deep to the upper layer:

$$\frac{\psi^p(y = L_0) - \psi_1^\dagger(y = -L_0)}{2L_0}\frac{g_1'}{h_1} \approx \frac{\kappa_1 g_1'}{h_1^2}, \tag{13}$$

   where we have used the buoyancy contrast g_i' defined by equation (8) and introduced the diapycnal mixing coefficient κ_i between layers i and $(i+1)$. This model allows for the topographic enhancement of the mixing coefficient by prescribing: $\kappa_1 < \kappa_2$. Combining equations (13), (1) and (11), we obtain the first dynamical balance of the model:

$$\frac{\varepsilon g_1' h_1^2}{4fL_0\Delta y} + \frac{K_{\text{eddy}} h_1}{2D_1 L_0} \approx \frac{\kappa_1}{h_1} + \frac{\tau_0}{2\rho_0 f_0 L_0}. \tag{14}$$

2. Vertically integrating from the abyssal to the deep layer yields:

$$\frac{0 - \psi_2^\dagger(y = -L_0)}{2L_0}\frac{g_2'}{h_2} \approx \frac{\kappa_2 g_2'}{h_2^2}. \tag{15}$$

   Combining equations (15), (1) and (11), we obtain the second dynamical balance of the model:

$$\frac{K_{\text{eddy}}(h_1 + h_2)}{2D_2 L_0} \approx \frac{\kappa_2}{h_2} + \frac{\tau_0}{2\rho_0 f_0 L_0}. \tag{16}$$

2.1.4. *Dimensionless equations*

Equations (14) and (16) can be simplified by introducing the following dimensionless numbers:

1. The dimensionless heights of each layer:

$$\tilde{h_i} \overset{\text{def}}{=} \frac{h_i}{H}. \tag{17}$$

2. The ratio of the two isopycnal outcrop's distances from the Northern edge of the circumpolar channel:

$$\delta \overset{\text{def}}{=} \frac{D_1}{D_2}. \tag{18}$$

3. The ratio of the two diapycnal diffusivities:

$$\tilde{\kappa} \overset{\text{def}}{=} \frac{\kappa_1}{\kappa_2}. \tag{19}$$

4. The typical ratio of the Ekman transport to the deep diffusive transport:

$$\tilde{\tau} \overset{\text{def}}{=} \frac{H}{2L_0}\frac{\tau_0}{\rho_0 f_0 \kappa_2}. \tag{20}$$

5. The typical ratio of the eddy-driven transport to the deep diffusive transport:

$$\tilde{K} \overset{\text{def}}{=} \frac{H^2}{2D_1 L_0}\frac{K_{\text{eddy}}}{\kappa_2}. \tag{21}$$

6. The typical ratio of the polar convective transport to the deep diffusive transport:

$$\tilde{B} = \frac{\varepsilon g_1' H^3}{4f_0 L_0 \kappa_2 \Delta y}. \tag{22}$$

The reference values for the parameters of the model are listed in table 1, and lead to the reference dimensionless numbers of the model listed in table 2. The equations become, dropping tildes:

$$\underbrace{Bh_1^2}_{\text{convection}} + \underbrace{Kh_1}_{\text{eddies}} = \underbrace{\tau}_{\text{wind}} + \underbrace{\frac{\kappa}{h_1}}_{\text{mixing}}, \tag{23}$$

$$\underbrace{K\delta(h_1 + h_2)}_{\text{eddies}} = \underbrace{\tau}_{\text{wind}} + \underbrace{\frac{1}{h_2}}_{\text{mixing}}. \tag{24}$$

2.1.5. *Mass conservation*

The dimensionless equations (23) and (24) are valid when the thickness of each layer is steady. To derive the dynamics of our model, we look at the incoming and outgoing transport of each layer on figure 1. The volume transport of a layer to another can be obtained by multiplying the streamfunctions by the zonal width W of our model, which we define to be the circumference of the Earth at the Northern edge of the circumpolar channel $W \overset{\text{def}}{=} a\cos(a^{-1}L_0)$:

$$\frac{dV_i}{dt} \approx S\frac{dh_i}{dt} \approx W(\psi_{\text{incoming}} - \psi_{\text{outgoing}}). \tag{25}$$

We have introduced the volume V_i of each layer and the surface S of the ocean. For instance, from the reference parameters listed in tables 1 and 2, the upper overturning cell transports 21Sv and the lower one 23Sv ($1\text{Sv} = 10^6 \text{m}^3.\text{s}^{-1}$). We are now able to write the dynamic version of equations (23) and (24) in dimensionless form; dropping tildes:

$$\dot{h}_1 = \underbrace{\tau}_{\text{wind}} + \underbrace{\frac{\kappa}{h_1}}_{\text{mixing}} - \underbrace{Kh_1}_{\text{eddies}} - \underbrace{Bh_1^2}_{\text{convection}}, \tag{26}$$

$$\dot{h}_2 = \underbrace{Kh_1}_{\text{eddies}} + \underbrace{Bh_1^2}_{\text{convection}} + \underbrace{\frac{1}{h_2}}_{\text{mixing}} - \underbrace{\frac{\kappa}{h_1}}_{\text{mixing}} - \underbrace{K\delta(h_1 + h_2)}_{\text{eddies}}, \tag{27}$$

$$\dot{h}_3 = \underbrace{K\delta(h_1 + h_2)}_{\text{eddies}} - \underbrace{\tau}_{\text{wind}} - \underbrace{\frac{1}{h_2}}_{\text{mixing}}. \tag{28}$$

In order to write (26), (27) and (28) in dimensionless form, we have defined the dimensionless derivative of a quantity X with

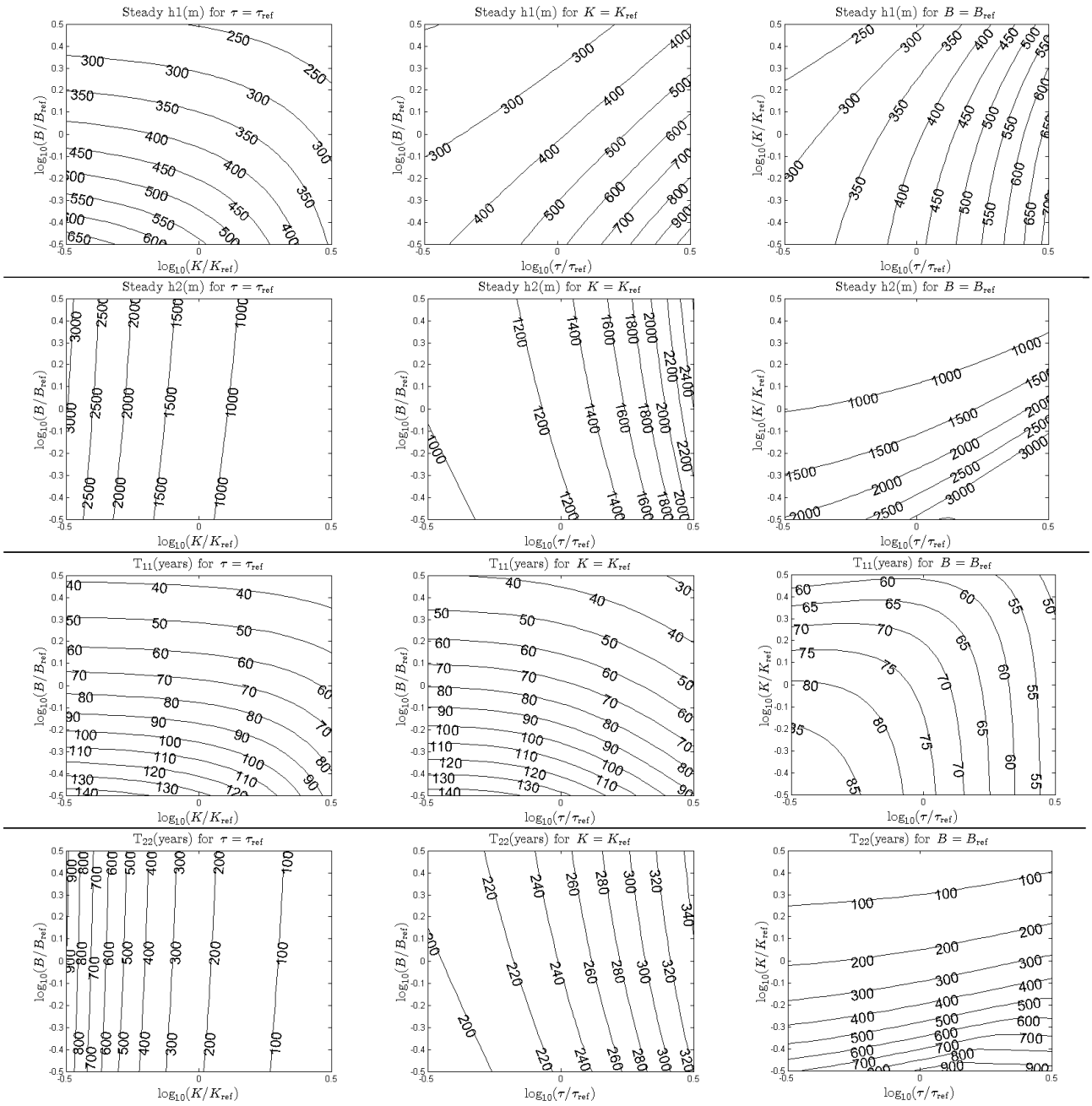

Figure 3. (Top to bottom) Steady thicknesses h_1, h_2; Linear adjustment timescales T_{11}, T_{22}
(Left to right) The variables are plotted in (K, B),(τ, B), (τ, K) parameter spaces. The other parameters are always held constant at their reference values listed in table 2.
The horizontal and vertical scales are logarithmic, and the center of each domain corresponds to the reference value.

respect to time:

$$\dot{X} \stackrel{\text{def}}{=} \frac{SH^2}{2WL_0\kappa_2}\frac{\partial X}{\partial t}, \tag{29}$$

where t is a dimensional measure of time. Note that these equations sum up to zero as by definition: $\dot{h_1} + \dot{h_2} + \dot{h_3} = \dot{1} = 0$, ie the total depth of the ocean is steady. Furthermore, equations (23) and (24) are respectively the steady versions of equations (26) and (28). These equations allow us to analytically diagnose the stratification (h_1, h_2, h_3) from a given set of oceanic parameters $(\tau, \kappa, K, B, \delta)$ in steady state. In the specific case where the diapycnal mixing coefficient increases sharply with depth ($\kappa_1 \ll \kappa_2 \Leftrightarrow \kappa \ll 1$), we can write simple expressions for the steady stratification:

$$h_1 = \frac{-K + \sqrt{K^2 - 4B\tau}}{2B}, \tag{30}$$

$$h_2 = \frac{\tau - K\delta h_1 + \sqrt{(\tau - K\delta h_1)^2 + 4K\delta}}{2K\delta}, \tag{31}$$

and $h_3 = 1 - h_1 - h_2$. In sections 2.2 and 2.3, we use the simple dynamics of the three layer model to gain insight into specific climate scenarios.

2.2. *Adjustment timescales of the three layer model*

We consider the following scenario: Starting from a state where the oceanic parameters $(\tau_{\text{old}}, \kappa_{\text{old}}, K_{\text{old}}, B_{\text{old}}, \delta_{\text{old}})$ produce a steady stratification $(h_{1\text{old}}, h_{2\text{old}}, h_{3\text{old}})$, a sudden change in the atmosphere/ocean makes the parameters instantly evolve to $(\tau, \kappa, K, B, \delta)$. The new parameters will make the stratification $(h_1(t), h_2(t), h_3(t))$ continuously evolve to a new value (h_1, h_2, h_3). For instance, if the wind stress increases from τ_a to τ_b, the new upper layer thickness h_1 will be thicker than $h_{1\text{old}}$ and the new abyssal thickness h_3 shallower than $h_{3\text{old}}$, and vice-versa. This evolution is entirely determined by equations (26), (27), (28), and the simplicity of these equations can help

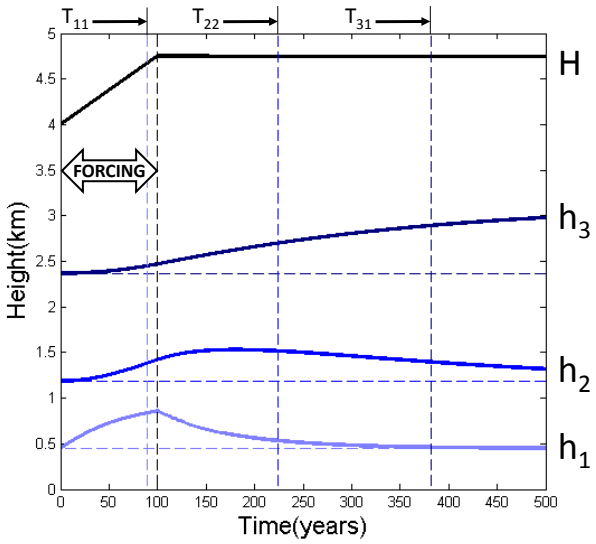

Figure 4. Evolution of the upper layer thickness h_1, deep layer thickness h_2, abyssal layer thickness h_3, and total thickness $H = h_1 + h_2 + h_3$ in time for a uniform warming of $1\mathrm{W.m}^{-2}$, applied for the first 100 years of the experiment.

understand the timescales of the evolution. If the perturbation of the system is small enough, ie $|h_2 - h_{2\mathrm{old}}| \ll 1$, the adjustment timescales can be approximated by their linear values:

$$T_{11} \overset{\text{def}}{=} -(\frac{\partial \dot{h}_1}{\partial h_1})^{-1}_{\mathrm{Eq}} = \frac{1}{\kappa h_1^{-2} + K + 2Bh_1} \overset{\kappa \ll 1}{\approx} (K^2 - 4B\tau)^{-\frac{1}{2}}, \tag{32}$$

$$T_{21} \overset{\text{def}}{=} (\frac{\partial \dot{h}_2}{\partial h_1})^{-1}_{\mathrm{Eq}} = \frac{1}{\kappa h_1^{-2} + K(1-\delta) + 2Bh_1} \overset{\kappa \ll 1}{\approx} \frac{1}{\sqrt{K^2 - 4B\tau} - K\delta}, \tag{33}$$

$$T_{22} = -(\frac{\partial \dot{h}_2}{\partial h_2})^{-1}_{\mathrm{Eq}} = \frac{1}{h_2^{-2} + K\delta}. \tag{34}$$

The dimensionless timescales T_{ij} represent the time it takes for the layer i to adjust to the perturbations of layer j; they must be multiplied by $SH^2(2WL_0\kappa_2)^{(-1)}$ to obtain a value in seconds, according to equation (29). The steady stratification and the linear timescales of the system as functions of (τ, K, B) are depicted on figure 3. The coupled timescales of the system can be found by computing the eigenvalues of the linear system, and taking the opposite of their inverse. The generality of these results make it possible to study the dynamical effect of any reasonable change of parameters (τ, κ, K, B) on the stratification and GOC (for instance the dynamical effect of a Southern wind increase on the stratification and the GOC).

2.3. *A simple heat uptake scenario*

Let us study the scenario where starting from equilibrium, the upper ocean is forced by a constant heat source, represented here by a mass source $\mathcal{F}$ (since our layers are defined by the position of the mean isopycnals, mass and heat conservations are analogous in our model):

$$\dot{h}_1 = \underbrace{\mathcal{F}}_{\text{forcing}} + \underbrace{\tau}_{\text{wind}} + \underbrace{\frac{\kappa}{h_1}}_{\text{mixing}} - \underbrace{Kh_1}_{\text{eddies}} - \underbrace{Bh_1^2}_{\text{convection}}. \tag{35}$$

Unlike the scenarios described in section 2.2, the total thickness of the ocean H is not conserved as: $\dot{H} = \mathcal{F}$ (ie the global ocean is warming/cooling). Let's take the example of a constant external warming $\mathcal{F} = 1\mathrm{W.m}^{-2}$ applied to the upper ocean for a century, which is depicted on figure 4. It increases the upper layer thickness with a typical time T_{11}, which causes an increase of the deep layer with a typical time T_{21}. Finally, the upper and lower layers will respectively warm up the abyssal layer of the ocean with timescales $(K\delta)^{-1}$ and $(K\delta + h_2^{-1})^{-1}$. When the forcing $\mathcal{F}$ stops, the thicknesses will not completely relax to their pre-forced equilibrium value with their dynamic timescales; there will be a recalcitrant component of the forcing, which mostly affects the abyssal layer (in the long term) in the example considered on figure 4.

3. Two-basin model of the global overturning circulation

3.1. *Model setup*

The model is a direct generalization of the single basin model presented in the previous section. It is depicted on figure 5 and contains three parts:

1. A basin identical to the one presented in the previous section (on the right) with three layers of thicknesses (h_{A1}, h_{A2}, h_{A3}) and a total depth H, which mimics the Atlantic basin.
2. A basin where waters do not convect near the North Pole (on the left) with three layers of thicknesses (h_{P1}, h_{P2}, h_{P3}) and a total depth H, analogous to the Indo-Pacific basin.
3. A circumpolar channel which transports water between the two basins.

We assume that the flow from one basin to another is geostrophic and generated by the difference of thicknesses between the two basins. Furthermore, as in section 2.1.2, we assume that the horizontal pressure gradients of the deep layers are negligible (see appendix A for a more rigorous approach), and that the abyssal layer is at rest (not likely to be a good approximation here). Combining equations (4) and (7), the transport generated by the difference in thickness between the two basins is:

$$\frac{1}{\Delta x}\int_{x_P}^{x_A} h_1 v_1 dx = \frac{g_1'}{f\Delta x}\int_{x_P}^{x_A} h_1 \frac{\partial h_1}{\partial x} dx = \frac{g_1'(h_{P1}^2 - h_{A1}^2)}{2f\Delta x}, \tag{36}$$

where $\Delta x = |x_A - x_P|$ is the distance between the eastern boundary density interface depths in each basin, located at (x_P, x_A). The sign of the transport comes from the fact that since the Pacific basin does not convect near the North Pole, its upper layer is thicker, which generates a transport from the Pacific to the Atlantic basin in the upper layer, and a transport from the Atlantic to the Pacific basin in the deep layer. If we make the equations dimensionless following the exact same procedure as in section 2.1.4, the dimensionless exchange transport is given by $\tilde{C}(\tilde{h}_{P1}^2 - \tilde{h}_{A1}^2)$. We have defined the typical dimensionless buoyancy gradient between the two basins:

$$\tilde{C} \overset{\text{def}}{=} \frac{g_1' H^3}{4f_0 L_0 \kappa_2 \Delta x} = \frac{\tilde{B}\Delta y}{\Delta x} = \mathrm{O}(\tilde{B}). \tag{37}$$

Since only half of the basins convect in the two basins model, we set $\varepsilon = 1/4$ in the definition of $\tilde{B}$ (22) for the two basin model. Generalizing equations (26), (27) and (28) can be done by considering the incoming and outgoing transports in each layer depicted on figure 5:

$$\frac{dV_{Ai}}{dt} \approx S_{\mathrm{Atl}}\frac{dh_{Ai}}{dt} \approx W_{\mathrm{Atl}}(\psi_{\mathrm{Atl,incoming}} - \psi_{\mathrm{Atl,outgoing}}), \tag{38}$$

$$\frac{dV_{Pi}}{dt} \approx S_{\mathrm{Pac}}\frac{dh_{Pi}}{dt} \approx W_{\mathrm{Pac}}(\psi_{\mathrm{Pac,incoming}} - \psi_{\mathrm{Pac,outgoing}}). \tag{39}$$

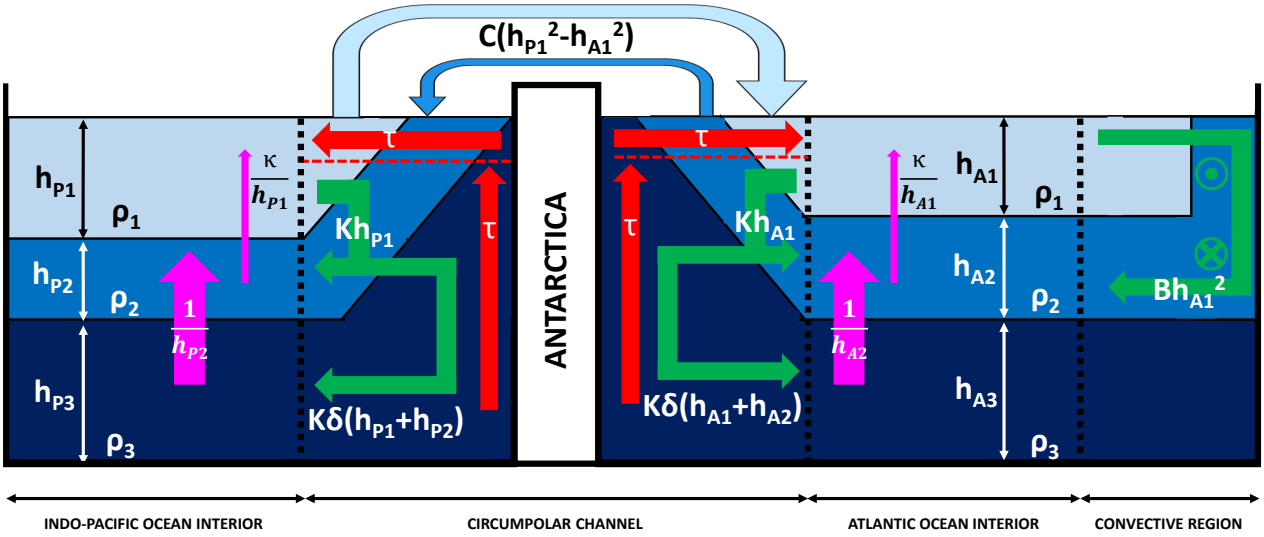

Figure 5. Two basins and three layer model of the global overturning circulation. The transports are indicated in dimensionless form.

We have distinguished the surface and with of the Atlantic basin $(S_{\rm Atl}, W_{\rm Atl})$ from their Indo-Pacific counterpart $(S_{\rm Pac}, W_{\rm Pac})$. Dropping tildes, the dynamics of the two basin three-layer model are:

$$\frac{\dot{h}_{A1}}{\sigma_A} = \underbrace{\tau}_{\text{wind}} - \underbrace{K h_{A1}}_{\text{eddies}} - \underbrace{B h_{A1}^2}_{\text{convection}} + \underbrace{\frac{\kappa}{h_{A1}}}_{\text{mixing}} + \underbrace{C(h_{P1}^2 - h_{A1}^2)}_{\text{exchange}}, \tag{40}$$

$$\begin{aligned}\frac{\dot{h}_{A2}}{\sigma_A} = &\underbrace{K h_{A1}}_{\text{eddies}} + \underbrace{B h_{A1}^2}_{\text{convection}} + \underbrace{\frac{1}{h_{A2}}}_{\text{mixing}} - \underbrace{\frac{\kappa}{h_{A1}}}_{\text{mixing}} \\ &- \underbrace{K\delta(h_{A1}+h_{A2})}_{\text{eddies}} - \underbrace{C(h_{P1}^2 - h_{A1}^2)}_{\text{exchange}},\end{aligned} \tag{41}$$

$$\frac{\dot{h}_{A3}}{\sigma_A} = \underbrace{K\delta(h_{A1}+h_{A2})}_{\text{eddies}} - \underbrace{\tau}_{\text{wind}} - \underbrace{\frac{1}{h_{A2}}}_{\text{mixing}}, \tag{42}$$

$$\frac{\dot{h}_{P1}}{\sigma_P} = \underbrace{\tau}_{\text{wind}} - \underbrace{K h_{P1}}_{\text{eddies}} + \underbrace{\frac{\kappa}{h_{P1}}}_{\text{mixing}} - \underbrace{C(h_{P1}^2 - h_{A1}^2)}_{\text{exchange}}, \tag{43}$$

$$\begin{aligned}\frac{\dot{h}_{P2}}{\sigma_P} = &\underbrace{K h_{P1}}_{\text{eddies}} + \underbrace{\frac{1}{h_{P2}}}_{\text{mixing}} - \underbrace{\frac{\kappa}{h_{P1}}}_{\text{mixing}} \\ &- \underbrace{K\delta(h_{P1}+h_{P2})}_{\text{eddies}} + \underbrace{C(h_{P1}^2 - h_{A1}^2)}_{\text{exchange}},\end{aligned} \tag{44}$$

$$\frac{\dot{h}_{P3}}{\sigma_P} = \underbrace{K\delta(h_{P1}+h_{P2})}_{\text{eddies}} - \underbrace{\tau}_{\text{wind}} - \underbrace{\frac{1}{h_{P2}}}_{\text{mixing}}. \tag{45}$$

We have defined the dimensionless aspect ratio of each basin:

$$\begin{pmatrix}\sigma_A \\ \sigma_P\end{pmatrix} \overset{\text{def}}{=} \frac{W}{S}\begin{pmatrix}S_{\rm Atl} W_{\rm Atl}^{-1} \\ S_{\rm Pac} W_{\rm Pac}^{-1}\end{pmatrix}. \tag{46}$$

Summing the previous equations, we can see that the total volume of each basin is conserved:

$$\dot{h}_{A1} + \dot{h}_{A2} + \dot{h}_{A3} = \dot{\sigma}_A = \dot{h}_{P1} + \dot{h}_{P2} + \dot{h}_{P3} = \dot{\sigma}_P = 0. \tag{47}$$

If we assume that all the basins have the same aspect ratio $(SW^{-1} = S_{\rm Atl} W_{\rm Atl}^{-1} = S_{\rm Pac} W_{\rm Pac}^{-1})$, then:

$$\sigma_A = \sigma_P = 1. \tag{48}$$

For example, (48) applies in the case where the basins are all identical. The steady version of equations (40), (41), (42), (43), (44) and (45) allows us to diagnose the steady stratification $(h_{A1}, h_{A2}, h_{A3}, h_{P1}, h_{P2}, h_{P3})$ for a given set of parameters: $(\tau, K, \kappa, \delta, B, C)$. The steady equations are coupled, nonlinear, and can not be solved analytically, except in specific limits where the Atlantic basin does not convect $(B \ll 1)$. The two basins are then identical and have the same stratification (h_1, h_2, h_3). The exchange term is zero and the problem reduces to solving the three layer model for two independent and identical single basins, which has already been done in section 2.

3.2. *Adjustment timescales*

Instead of the four linear timescales of section 2.2, the system now has sixteen timescales! The most relevant timescales to capture the evolution of the upper and lower layer of each basin are the intrinsic timescales of each layer:

$$T_{A1A1} = -(\frac{\partial \dot{h}_{A1}}{\partial h_{A1}})_{\rm Eq}^{-1} = \frac{\sigma_A}{\kappa h_{A1}^{-2} + K + 2(B+C)h_{A1}}, \tag{49}$$

$$T_{A2A2} = (\frac{\partial \dot{h}_{A2}}{\partial h_{A2}})_{\rm Eq}^{-1} = \frac{\sigma_A}{h_{A2}^{-2} + K\delta}, \tag{50}$$

$$T_{P1P1} = -(\frac{\partial \dot{h}_{P1}}{\partial h_{P1}})_{\rm Eq}^{-1} = \frac{\sigma_P}{\kappa h_{P1}^{-2} + K + 2C h_{P1}}, \tag{51}$$

$$T_{P2P2} = (\frac{\partial \dot{h}_{P2}}{\partial h_{P2}})_{\rm Eq}^{-1} = \frac{\sigma_P}{h_{P2}^{-2} + K\delta}. \tag{52}$$

These timescales are very similar to the timescales of the one basin model, given by equations (32) and (34). In order to compare the difference between the one and two basin(s) model, we test the influence of an instantaneous doubling of the Southern wind stress $\tilde{\tau}_{\rm ref} \mapsto 2\tilde{\tau}_{\rm ref}$ on the stratification and the GOC. On figure 6, we can see that the stratification predicted by the one basin model lies between the stratification of the two basins for all time, and is closer to the Atlantic stratification. The adjustment timescales of the one basin model (T_{11}, T_{22}) roughly indicate when the stratification is halfway through its evolution to the new equilibrium. Finally, the one and two basins model agree (the difference is smaller than ± 1Sv) on the fact that the GOC transport evolves from 20Sv to 39Sv.

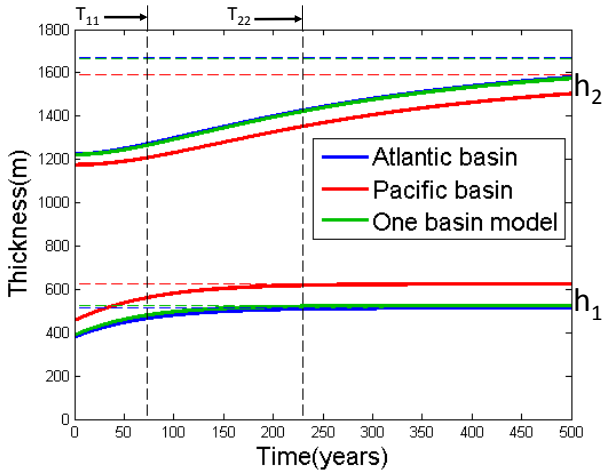

Figure 6. Evolution of the stratification in time for a doubling of the Southern winds from $\tilde{\tau}_{\rm ref}$ to $2\tilde{\tau}_{\rm ref}$, while the other parameters are maintained at their reference values. The new equilibrium stratification is indicated by dotted horizontal lines. The two adjustment timescales (T_{11}, T_{22}) are indicated by vertical dotted lines.

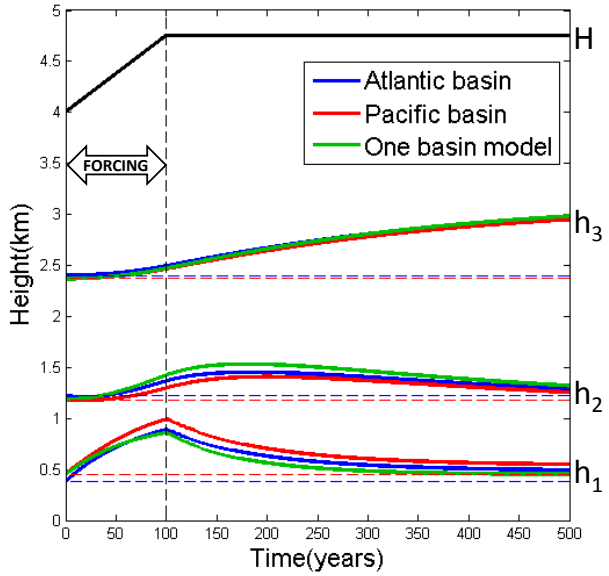

Figure 7. Evolution of the stratification in time for a uniform warming of $1\mathrm{W.m}^{-2}$, applied for the first 100 years of the experiment. The initial stratification is indicated by horizontal dotted lines.

3.3. Simple heat uptake experiment

We repeat the simple heat uptake experiment of section 2.3, imposing the forcing to both Atlantic and Indo-Pacific basins, by adding $\mathcal{F} > 0$ to the right hand side of equations (40) and (43). The evolution of the stratification in the two basins model is once again compared to its counterpart in the one basin model on figure 7. We observe two differences:

1. The stratification of the upper/deep layer increases more/less in the two basins than in the one basin model, while the evolution of the abyssal stratification is almost identical. This can be explained by the sensitivity of the long term equilibrium solution to a change in wind stress $\tilde{\tau}$ (the forcing $\mathcal{F}$ is comparable to the wind stress in our equations because it is independent of the stratification). The increased sensitivity of the upper layer $(\partial h_{1,\rm eq}/\partial\tau)$ and decreased sensitivity of the deep layer $(\partial h_{2,\rm eq}/\partial\tau)$ is linked to the fact that convection only happens in one basin in the two basins model.
2. The adjustment timescales are slightly shorter in the two basins model. Because of the nonlinearity of the exchange transport $\tilde{C}(\tilde{h}_{P1}^2 - \tilde{h}_{A1}^2)$, the latter is amplified by the forcing $\mathcal{F}$ over time: Typically, for a time lapse Δt , the exchange transport will be $\sim 2\tilde{C}(\tilde{h}_{P1} - \tilde{h}_{A1})\mathcal{F}\Delta t$ larger than its unforced equivalent, decreasing the adjustment timescales of the coupled two basins system.

4. Conclusion

We have developed a simple one basin and two basins three layer model of the GOC. In this model, the oceanic stratification evolves in response to the parameters $(\tau, K, \kappa, \delta, B, C)$, respectively defined by equations (20), (21), (19), (18), (22) and (37). If any of these processes change, the stratification and the GOC evolve, approximately following the adjustment timescales T_{11} (equation (32)) and T_{22} (equation (34)). These timescales also help us understand how the GOC uptakes heat. The first and second layer absorb heat with their intrinsic timescales, and eventually transfer the heat to the thick abyssal layer with the deep Southern eddies turnover timescale. This model of heat uptake is analogous to (Marshall and Zanna 2014); both models are based on water-mass transformation and offer a physical alternative to the "upwelling diffusion" paradigm, and the box models currently used to analyze the outputs of coupled atmosphere-ocean GCM. Finally, when we allow the zonal inter-basin exchange between a mixing-driven basin with a thick/shallow upper/deep layer and a convectively-driven basin with a shallow/thick upper/deep layer, we observe two main differences:

1. The timescales of the coupled system are shortened (eg equation (49)).
2. The upper/deep layer responds more/less to a positive forcing, for instance in the case of a warming of the upper ocean.

It is important to remember that we have made several simplifying assumptions which may limit the validity of our model in certain situations. We have implicitly taken into account fixed atmospheric buoyancy boundary conditions by prescribing the latitude at which the mean isopycnals outcrop. In reality, there is an unsteady combination of fixed and relaxation atmosphere-ocean buoyancy fluxes. Despite the fact that the deep layer is only a few times larger than the upper one in our model, we have assumed that the upper layer was so thin that its velocity was much larger than the deep layer's one. We have neglected the inter-basin geostrophic transport in the abyssal layer, which is a big approximation since this layer outcrops in the circumpolar channel. We have chosen a simple closure for the baroclinic eddies and the model exhibits a strong sensitivity to the closure constant, which needs to be tested against an eddy-permitting model. By adopting a simple rectangular basin geometry, we have neglected the dynamical effects of the Drake Passage and the Mid-Atlantic ridges. We have not separated the effects of heat and salt in the buoyancy fluxes, preventing the multiple equilibria of the thermohaline circulation (eg (Johnson and Marshall 2007)).

The simplicity of this model could make it a keystone for future work, for example one could:

1. Analyze the outputs of two typical GCM experiments: An increase of the Southern winds, and a heat uptake or an oceanic cooling experiment.
2. Simply model the oceanic carbon cycle.
3. Simply model the coupling of the sea-ice oscillations to the GOC.
4. Study the glacial/interglacial problem.

A. Polar convective transport for upper and deep layers of similar velocities

If we do not make the thin upper layer approximation, which is necessary to write equation (7), then the horizontal pressure

gradients of the deep layer are not negligible anymore:

$$p_2(x,y,z) = \rho_0\varphi(x,y) - \rho_2 g z, \tag{53}$$

where φ is a potential to be determined. Applying the dynamical condition at the interface between the upper and deep layer, the pressure in the upper layer is given by:

$$p_1(x,y,z) = \rho_0 g_1' h_1(x,y) + \rho_0\varphi(x,y) - \rho_1 g z. \tag{54}$$

Combining equations (4) and (6), we can eliminate $\varphi(x,y)$ from the dynamics, yielding:

$$h_1 u_1 = -h_2 u_2 = -\frac{g_1'}{f}\frac{h_1 h_2}{h_1+h_2}\frac{\partial h_1}{\partial y}. \tag{55}$$

The total dimensionless circulation at $(y = L_0)$ then becomes:

$$\tilde{B}\tilde{h}_1^2 \to \tilde{B}\tilde{h}_1^2\frac{\tilde{h}_2}{\tilde{h}_1+\tilde{h}_2}. \tag{56}$$

Following the same reasoning, we can correct the transport generated by the zonal thickness gradient (36) to obtain a more rigorous dimensionless exchange transport:

$$\tilde{C}(\tilde{h}_{P1}^2 - \tilde{h}_{A1}^2) \to 2\tilde{C}\int_{x_P}^{x_A}\frac{\tilde{h}_1\tilde{h}_2}{\tilde{h}_1+\tilde{h}_2}\frac{\partial\tilde{h}_1}{\partial x}dx \tag{57}$$

References

Allison, L. C., Johnson, H. L., & Marshall, D. P. (2011). Spin-up and adjustment of the Antarctic Circumpolar Current and global pycnocline. Journal of Marine Research, 69(2), 167189. doi:10.1357/002224011798765330

Frolicher, T., Sarmiento, J., Paynter, D., Dunne, J., & Winton, M. (2014). Anthropogenic carbon and heat uptake in CMIP5 models : The dominance of the Southern Ocean, 16, 10567. doi:10.1175/JCLI-D-14-00117.1

Furst, J. J., & Levermann, A. (2011). A minimal model for wind- and mixing-driven overturning: threshold behavior for both driving mechanisms. Climate Dynamics, 38(1-2), 239260. doi:10.1007/s00382-011-1003-7

Ganachaud, a, & Wunsch, C. (2000). Improved estimates of global ocean circulation, heat transport and mixing from hydrographic data. Nature, 408(6811), 453–457. doi:10.1038/35044048

Ganachaud, A., & Wunsch, C. (2003). Large-scale ocean heat and freshwater transports during the world ocean circulation experiment. Journal of Climate, 16(4), 696–705. doi:10.1175/1520-0442(2003)016<0696:LSOHAF>2.0.CO;2

Ganachaud, A. (2003). Large-scale mass transports, water mass formation, and diffusivities estimated from World Ocean Circulation Experiment (WOCE) hydrographic data. Journal of Geophysical Research, 108(C7). doi:10.1029/2002JC001565

Gent, P. R., & McWilliams, J. C. (1990). Isopycnal Mixing in Ocean Circulation Models. Journal of Physical Oceanography. doi:10.1175/1520-0485(1990)020<0150:IMIOCM>2.0.CO;2

Gildor, H., Tziperman, E., & Toggweiler, J. R. (2002). Sea ice switch mechanism and glacial-interglacial CO2 variations. Global Biogeochem. Cycles, 16(3), 1032–. doi:10.1029/2001gb001446

Gnanadesikan, a. (1999). A Simple Predictive Model for the Structure of the Oceanic Pycnocline. doi:10.1126/science.283.5410.2077

Held, I. M., Winton, M., Takahashi, K., Delworth, T., Zeng, F., & Vallis, G. K. (2010). Probing the Fast and Slow Components of Global Warming by Returning Abruptly to Preindustrial Forcing. Journal of Climate, 23(9), 24182427. doi:10.1175/2009JCLI3466.1

Ito, T., & Follows, M. J. (2013). Air-sea disequilibrium of carbon dioxide enhances the biological carbon sequestration in the Southern Ocean. Global Biogeochemical Cycles, 27(4), 1129–1138. doi:10.1002/2013GB004682

Johnson, H. L., Marshall, D. P., & Sproson, D. A. J. (2007). Reconciling theories of a mechanically driven meridional overturning circulation with thermohaline forcing and multiple equilibria. Climate Dynamics, 29(7-8), 821836. doi:10.1007/s00382-007-0262-9

Jones, D. C., Ito, T., & Lovenduski, N. S. (2011). The transient response of the Southern Ocean pycnocline to changing atmospheric winds. Geophysical Research Letters, 38(15). doi:10.1029/2011GL048145

Kostov, Y., Armour, K. C., & Marshall, J. (2014). Impact of the Atlantic meridional overturning circulation on ocean heat storage and transient climate change. Geophysical Research Letters, 41(6), 21082116. doi:10.1002/2013GL058998

Lumpkin, R., & Speer, K. (2007). Global Ocean Meridional Overturning. Journal of Physical Oceanography, 37(10), 2550–2562. doi:10.1175/JPO3130.1

Luyten, J. R., Pedlosky, J., & Stommel, H. (1983). The Ventilated Thermocline. Journal of Physical Oceanography, 13(2), 292309. doi:10.1175/1520-0485(1983)013<0292:TVT>2.0.CO;2

Maier-Reimer, E. (1993). Geochemical cycles in an ocean general circulation model. Preindustrial tracer distributions. Global Biogeochemical Cycles, 7(3), 645–677. doi:10.1029/93GB01355.

Marshall, J., & Radko, T. (2003). Residual-Mean Solutions for the Antarctic Circumpolar Current and Its Associated Overturning Circulation. Journal of Physical Oceanography, 33(11), 2341–2354. doi:10.1175/1520-0485(2003)033<2341:RSFTAC>2.0.CO;2

Marshall, J., Scott, J. R., Armour, K. C., Campin, J. M, Kelley, M., & Romanou, A. (2015). The oceans role in the transient response of climate to abrupt greenhouse gas forcing. Clim Dyn, 44, 22872299. doi:10.1007/s00382-014-2308-0

Marshall, J., & Speer, K. (2012). Closure of the meridional overturning circulation through Southern Ocean upwelling. Nature Geoscience, 5(3), 171180. doi:10.1038/ngeo1391

Marshall, D. P., & Zanna, L. (2014). A Conceptual Model of Ocean Heat Uptake under Climate Change. Journal of Climate, 27(22), 84448465. doi:10.1175/JCLI-D-13-00344.1

A. Mashayek, R. Ferrari, M. Nikurashin, and W. R. Peltier, 2015: Influence of Enhanced Abyssal Diapycnal Mixing on Stratification and the Ocean Overturning Circulation. J. Phys. Oceanogr., 45, 25802597. doi: http://dx.doi.org/10.1175/JPO-D-15-0039.1

Nikurashin, M., & Vallis, G. (2011). A Theory of Deep Stratification and Overturning Circulation in the Ocean. Journal of Physical Oceanography, 41(3), 485–502. doi:10.1175/2010JPO4529.1

Nikurashin, M., & Vallis, G. (2012). A Theory of the Interhemispheric Meridional Overturning Circulation and Associated Stratification. Journal of Physical Oceanography, 42(10), 1652–1667. doi:10.1175/JPO-D-11-0189.1

Plumb, R. A., & Ferrari, R. (2005). Transformed Eulerian-Mean Theory. Part I: Nonquasigeostrophic Theory for Eddies on a Zonal-Mean Flow. Journal of Physical Oceanography, 35(2), 165–174. doi:10.1175/JPO-2669.1

Raper, S. C. B., Gregory, J. M., & Stouffer, R. J. (2002). The role of climate sensitivity and ocean heat uptake on AOGCM transient temperature response. Journal of Climate, 15(1), 124130. doi:10.1175/1520-0442(2002)015<0124:TROCSA>2.0.CO;2

Shakespeare, C. J., & McC. Hogg, A. (2012). An analytical model of the response of the meridional overturning circulation to changes in wind and buoyancy forcing. Journal of Physical Oceanography, 42(8), 12701287. doi:10.1175/JPO-D-11-0198.1

Talley, L. D. (2013). Closure of the Global Overturning Circulation Through the Indian, Pacific, and Southern Oceans: Schematics and Transports. OCEANOGRAPHY, 26(1), 80–97. doi:10.5670/oceanog.2013.07

Talley, L. D. (2008). Freshwater transport estimates and the global overturning circulation: Shallow, deep and throughflow components. Progress in Oceanography, 78(4), 257–303. doi:10.1016/j.pocean.2008.05.001

Toggweiler, J. R. (1999). Variation of atmospheric CO2 by ventilation of the ocean's deepest water. Paleoceanography. doi:10.1029/1999PA900033

Vallis, G. K. (2006). Athmospheric and oceanic fluid dynamics, Fundamental and large-scale circulation. Cambridge University Press. doi:10.2277/0521849691

Waterhouse, A. F., MacKinnon, J. a., Nash, J. D., Alford, M. H., Kunze, E., Simmons, H. L., … Lee, C. M. (2014). Global Patterns of Diapycnal Mixing from Measurements of the Turbulent Dissipation Rate. Journal of Physical Oceanography, 44(7), 1854–1872. doi:10.1175/JPO-D-13-0104.1

Winton, M., Takahashi, K., & Held, I. M. (2010). Importance of Ocean Heat Uptake Efficacy to Transient Climate Change. Journal of Climate, 23(9), 2333–2344. doi:10.1175/2009JCLI3139.1

Parameter	Description	Value
a	Radius of the Earth	$6.4.10^3$km
D_1	Mean Isopycnal outcrop - Northern edge of the channel	$1.1.10^3$km (10°)
D_2	Second Isopycnal outcrop - Northern edge of the channel	$1.4.10^3$km (12.5°)
f_0	Coriolis parameter at the Northern edge of the basin	$1.1.10^{-4}$s^{-1} (50°)
g	Gravity constant	9.8m.s^{-2}
g_2'	Reduced gravity between the deep and abyssal layers	2.10^{-2}m.s^{-2}
H	Mean ocean depth	4.0km
K_{eddy}	Lateral eddy diffusivity in the channel	1.10^3m^2.s^{-1}
L	Quarter of the Earth's perimeter	$1.0.10^4$km (90°)
L_0	Northern edge of the channel - Equator	$6.1.10^3$km (50°)
S	Total surface of the ocean	$3.5.10^{14}$m^2
W	Circumference of the Earth at the Drake passage	$2.6.10^4$km (50°)
Δx	South Eastern Pacific - South Eastern Atlantic	2.10^6km
Δy	Extent of the polar buoyancy gradient	2.10^6km
ε	Fraction of the ocean open to the polar convective zone	1/8 (45°/360°)
κ_1	Diapycnal diffusivity in the upper/deep layer	$1.0.10^{-5}$m^2.s^{-1}
κ_2	Diapycnal diffusivity in the abyssal layer	$1.0.10^{-4}$m^2.s^{-1}
ρ_0	Reference density of the ocean	$1.0.10^3$kg.m^{-3}
τ_0	Wind stress at the Northern edge of the channel	0.10Pa

Table 1. Reference dimensional parameters

Parameter	Definition	Reference Value
B_{ref}	22	323 (1 basin)/645 (2 basins)
C_{ref}	37	645
K_{ref}	21	13
δ_{ref}	18	1.25
κ_{ref}	19	0.1
σ_A	46	1
σ_P	46	1
τ_{ref}	20	3

Table 2. Reference dimensionless parameters